Multiple phase transitions in networks of directed networks

Xueming Liu,[1,2] Linqiang Pan,[1] H. Eugene Stanley,[2] and Jianxi Gao[3,*]

[1]*Key Laboratory of Image Information Processing and Intelligent Control, School of Automation,*
Huazhong University of Science and Technology, Wuhan 430074, Hubei, China
[2]*Department of Physics, Center for Polymer Studies, Boston University, Boston, Massachusetts 02215, USA*
[3]*Department of Computer Science, Rensselaer Polytechnic Institute, Troy, New York 12180, USA*

The robustness in real-world complex systems with dependency connectivities differs from that in isolated networks. Although most complex network research has focused on interdependent undirected systems, many real-world networks—such as gene regulatory networks and traffic networks—are directed. We thus develop an analytical framework for examining the robustness of networks made up of directed networks of differing topologies. We use it to predict the phase transitions that occur during node failures and to generate the phase diagrams of a number of different systems, including treelike and random regular (RR) networks of directed Erdős-Rényi (ER) networks and scale-free networks. We find that the the phase transition and phase diagram of networks of directed networks differ from those of networks of undirected networks. For example, the RR networks of directed ER networks show a hybrid phase transition that does not occur in networks of undirected ER networks. In addition, system robustness is affected by network topology in networks of directed networks. As coupling strength q increases, treelike networks of directed ER networks change from a second-order phase transition to a first-order phase transition, and RR networks of directed ER networks change from a second-order phase transition to a hybrid phase transition, then to a first-order phase transition, and finally to a region of collapse. We also find that heterogenous network systems are more robust than homogeneous network systems. We note that there are multiple phase transitions and triple points in the phase diagram of RR networks of directed networks and this helps us understand how to increase network robustness when designing interdependent infrastructure systems.

I. INTRODUCTION

Complex networks have been widely used to model interconnected systems in fields ranging from the power grid [1,2] to the Internet [3–6], to social and biological systems [7–10]. In these complex networks, node or link failures can occur. The ability of networks to retain their connectivity under link or node failures is called network robustness [11–16]. The robustness of a complex network can be determined either by the integral size of the giant component during the attacking process or by the percolation threshold [17–21]. The percolation threshold p_c is the minimal fraction of remaining nodes or links needed to maintain network connectivity and is usually predicted using percolation theory from statistical physics [3]. Most studies on the robustness of complex networks have focused on single or isolated networks [6].

Critical infrastructures in the real world interact with each other and form a network of interdependent networks [13,16,19,22–33]. In interdependent networks, the failure of a node in one network causes the failure of dependent nodes in other networks, which, in turn, can cause further damage to the first network, leading to cascading failures and possible catastrophic consequences. For example, the breakdown of an interdependent communication network and a power grid

caused the electrical blackout that affected much of Italy on 28 September 2003 [34]. To study complex network interdependence, Buldyrev *et al.* [13] developed a fundamental framework of two fully interdependent networks that can be theoretically analyzed using a generating function formalism [35] and discovered a first-order discontinuous phase transition that differs dramatically from the second-order continuous phase transition found in isolated networks [36,37]. Pashani *et al.* [23] studied a more realistic model of two partially interdependent networks and found a change from a first-order phase transition to a second-order phase transition when the coupling strength between the networks decreases. In addition, a systematic series of mathematical frameworks has been proposed to analyze the robustness of networks of more than two interdependent networks [15,19,38–42].

All of these studies focus on undirected networks, but many real-world networks are directed, including metabolic networks and gene regulatory networks in biological systems [9,43], transportation networks, and power grids in infrastructure systems [44,45], and citation networks and trust networks in social systems [46,47]. Recently Azimi-Tafreshi *et al.* [48] studied giant components in directed multiplex networks and found that a giant strongly connected component (GSCC) is more vulnerable that a giant weakly connected component. Although we have developed a theoretical framework for analyzing the robustness of two interdependent directed networks with arbitrary degree distributions and have applied

*Corresponding author: gaoj8@rpi.edu

it to real international trade networks [49], we still do not have a framework for studying the robustness in networks of directed networks of more than two interdependent networks.

We here build a model of networks of directed networks (NODNs) and develop a general theoretical framework for analyzing NODNs with different topologies. We use it to calculate the percolation thresholds—p_c^{I} for first-order phase transitions and p_c^{II} for second-order phase transitions—that characterize system robustness and analyze the systemic phase diagrams divided by the critical coupling strengths, q_{c2} that separates the second and hybrid phases, q_{c1} that separates the hybrid and first phases, and q_{max} that separates the first and collapsed regions. The following findings will enable us to understand system robustness and design more robust infrastructures.

(i) The phase transitions in NODNs differ from those in networks of undirected networks. For example, random regular (RR) networks of directed Erdős-Rényi (ER) networks show a hybrid phase transition not present in networks of undirected ER networks.

(ii) System robustness in networks of directed networks is affected by network topology. The treelike structure of directed networks changes from a second-order phase transition to a first-order phase transition as coupling strength q increases. RR networks of directed networks exhibit a second-order phase transition when the coupling strength is $q < q_{c2}$, a hybrid phase transition when $q_{c2} < q < q_{c1}$, a first-order phase transition when $q_{c1} < q < q_{max}$, and a complete collapse when $q > q_{max}$.

(iii) In RR networks of directed scale-free (SF) networks, systems of heterogeneous networks are more robust than systems of homogenous networks.

(iv) We find triple points in the phase diagrams of both RR networks of ER and SF networks, which indicate ways of pushing the interdependent system into a safe region to prevent system collapse.

II. MODEL

Our NODN model is a network of n interdependent directed networks in which each node i ($i = 1, 2, \ldots, n$) is a network containing N_i nodes connected by directed connectivity links, and each link indicates a fully or partially dependent pair of networks. A NODN may have a treelike structure with no loops [see Figs. 1(a)–1(c)] or a random regular structure with loops [see Figs. 1(d) and 1(e)]. Networks i and j are connected by a dependency link when there is a $q_{ij} > 0$ fraction of nodes in network i that depends on nodes in network j or a $q_{ji} > 0$ fraction of nodes in network j that depends on nodes in network i [see Fig. 1(f)]. Nodes in one network stop functioning when nodes on which they are dependent in a second network stop functioning. In addition, the nodes from two networks are coupled under the "no-feedback" condition [19]. A node in one network can depend on only one node in a second network. Thus when node a in network i depends on node b in network j and node b in network j depends on node c in network i, then $a = c$. We assume that a node remains functional if it has not been removed and belongs to the GSCC. This assumption can cause cascading failures between networks. Nodes in network i
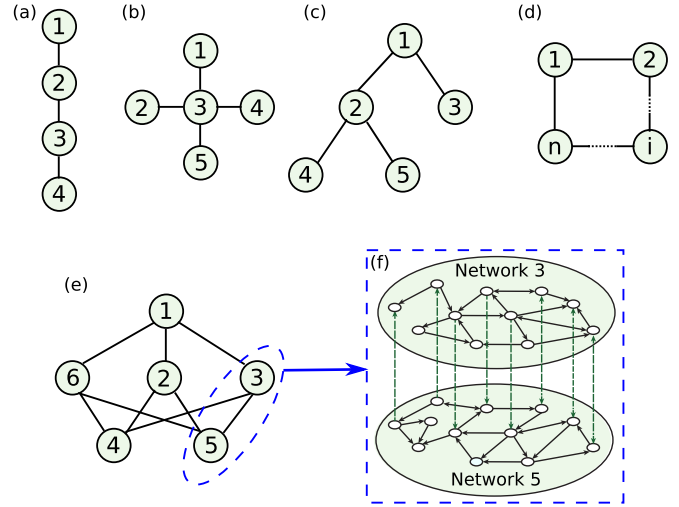

FIG. 1. Schematic of NODNs. (a)–(c) are treelike NODNs without loops. (d) and (e) are random regular NODNs with loops. (f) A partially dependent pair of two directed networks: network 3 and network 5 are coupled by directed dependency links (dotted green lines) with a no-feedback condition [19]. A dotted directed line from node i in one network to node j in the other network indicates that a failure of node i will cause node j to fail. There is a fraction $q_{35} = 5/11$ of nodes in network 3 that depend on the nodes of network 5, and the $q_{53} = 6/12$ fraction of nodes in network 5 depends on the nodes of network 3.

fail when they do not belong to the GSCC, and these failed nodes cause dependent nodes in other networks to also fail. This may divide the networks into components and cause more failures of nodes not in the GSCC, which can cause further failures back in the nodes in network i. This process continues iteratively until failures are no longer possible, and the surviving nodes in all networks form a final GSCC in the NODN.

III. ANALYTIC FRAMEWORK OF THE DYNAMIC PROCESS OF CASCADING FAILURES

The N_i nodes of network i are connected following a joint degree distribution $P_i(k_{in}, k_{out})$, where k_{in} and k_{out} are the in degree and out degree of a given node, respectively. Each network i can be characterized by a generating function [50,51],

$$\Phi_i(x, y) = \sum_{k_{in}, k_{out}}^{\infty} P_i(k_{in}, k_{out}) x^{k_{in}} y^{k_{out}}, \tag{1}$$

where x and y are arbitrary complex variables. The generating functions for the branching processes [50,51] are

$$\Phi_{i1}(x, 1) = \frac{\partial_y \Phi_i(x, y)|_{y=1}}{\partial_y \Phi_i(1, 1)}, \quad \Phi_{i1}(1, y) = \frac{\partial_x \Phi_i(x, y)|_{x=1}}{\partial_x \Phi_i(1, 1)}. \tag{2}$$

To compute the size of the GSCC in network i, we define a generating function [49],

$$\Phi_i^{(s)}(x, y) = \Phi_i(x, 1) + \Phi_i(1, y) - \Phi_i(x, y). \tag{3}$$

When a fraction $1 - p$ of nodes is randomly removed from network i, the relative size of the GSCC in the remaining network [50] is

$$g_i(p) = 1 - \Phi_i^{(s)}[px_c(p) + 1 - p, py_c(p) + 1 - p], \quad (4)$$

where $x_c(p)$ and $y_c(p)$, respectively, satisfy

$$x_c(p) = \Phi_{i1}[px_c(p) + 1 - p, 1],$$
$$y_c(p) = \Phi_{i1}[1, py_c(p) + 1 - p]. \quad (5)$$

To compute the size of the final GSCC we analyze the the cascading failure dynamics step by step. At $t = 1$ we randomly remove a fraction $1 - p_i$ of nodes from each network i after which the remaining fraction of nodes of each network i is $\psi'_{i,1} \equiv p_i$ and the remaining functional part is $\psi_{i,1} = \psi'_{i,1}g_i(\psi'_{i,1})$. Since the dependency links between networks follow the no-feedback condition, the damage spreading from network i to network j at step $t - 1$ does not spread back from network j to network i at step t. We define $r_{ij,t}$ as the fraction of remaining nodes in network i after the damage from all networks connected to i, denoted $\mathcal{N}_i$, except network j ($j \in \mathcal{N}_i$) at time step t. At time step $t = 1$ each network i receives damage from initial failures $1 - p_i$ but no damage from other networks. Thus $r_{ij,1} = p_i$ for $j \in \mathcal{N}_i$. At time step $t > 1$ each network i receives damage from all of its neighboring networks. The damage from a neighbor network j ($j \in \mathcal{N}_i$) to network i is $q_{ji}[1 - r_{ji,t-1}g_j(\psi'_{j,t-1})]$. Thus the fraction of the remaining nodes in network i at step t is

$$\psi'_{i,t} = p_i \prod_{j \in \mathcal{N}_i} \{1 - q_{ji}[1 - r_{ji,t-1}g_j(\psi'_{j,t-1})]\}, \quad (6)$$

and according to the definition of $r_{ij,t}$, it satisfies

$$r_{ij,t} = \frac{\psi'_{i,t}}{1 - q_{ji}[1 - r_{ji,t-1}g_j(\psi'_{j,t-1})]}. \quad (7)$$

At time step t, the fraction of the remaining functional part of network i is $\psi_{i,t} = \psi'_{i,t}g_i(\psi'_{i,t})$.

At the end of the cascading failure process the system is in a stationary state, and no more failures occur. If the system reaches a stationary state at step τ, then the fraction of the remaining nodes is $\psi'_{i,\tau} = \psi'_{i,\tau+1}$ for each network i. Thus the stationary state of the system satisfies the n equations,

$$\psi'_{i,\tau} = p_i \prod_{j \in \mathcal{N}_i} \{1 - q_{ji}[1 - r_{ji,\tau}g_j(\psi'_{j,\tau})]\}, \quad (8)$$

where $i = 1, 2, \ldots, n$ and

$$r_{ij,\tau} = \frac{\psi'_{i,\tau}}{1 - q_{ji}[1 - r_{ji,\tau}g_j(\psi'_{j,\tau})]}. \quad (9)$$

For each network i, the relative size of the final GSCC in the full complex network is

$$p^{(s)}_{\infty,i} = \psi'_{i,\tau}g_i(\psi'_{i,\tau}). \quad (10)$$

Note that, if $n = 2$, then $r_{12,\tau} = p_1$, $r_{21,\tau} = p_2$, and the n equations [Eq. (8)] can be simplified into two equations: $\psi'_{1,\tau} = p_1[p_2q_{21}g_2(\psi'_{2,\tau}) - q_{21} + 1]$ and $\psi'_{2,\tau} = p_2[p_1q_{12}g_1(\psi'_{1,\tau}) - q_{12} + 1]$, which is in accord with the result of two interdependent directed networks [49]. We

next calculate the stationary states of NODNs with differing topologies: treelike NODNs and random regular NODNs.

IV. TREELIKE NETWORKS OF INTERDEPENDENT DIRECTED NETWORKS

Generally speaking, all NODNs with a topology without loops are treelike. For example, interdependent network systems with linelike [Fig. 1(a)], starlike [Fig. 1(b)], and treelike [Fig. 1(c)] structures are all treelike NODNs. We examine a simplification that can be solved analytically: A treelike NODN in which each pair of connected networks is fully interdependent, i.e., $q_{ij} = 1$ for $i = 1, 2, \ldots, n$ and $j = 1, 2, \ldots, n$. We simplify Eq. (9) to $r_{ji,\tau} = \psi'_{j,\tau}/r_{ij,\tau}g_i(\psi'_{i,\tau})$. Similarly $r_{ij,\tau} = \psi'_{i,\tau}/r_{ji,\tau}g_j(\psi'_{j,\tau})$. These two equations yield $\psi'_{i,\tau}g_i(\psi'_{i,\tau}) = \psi'_{j,\tau}g_j(\psi'_{j,\tau}) = p^{(s)}_\infty$, where $p^{(s)}_\infty$ is the size of the final GSCC, which is the same for every network in the treelike NODN.

Because the nodes of each pair of fully interdependent networks are connected following the no-feedback condition, every node of one network can reach one node of any other network via a path consisting of dependency links, and there is no crossing between the dependency paths. When a node in one network fails, all the nodes on its dependency link path also fail. Thus initial attacks on the fraction of nodes $1 - p_i$ in each network i are equivalent to initial attacks on a fraction of nodes $1 - \prod_{i=1}^n p_i$ in one network. In addition, by calculating the values of $r_{ij,\tau}$ one by one, we get the size of the final GSCC,

$$p^{(s)}_\infty = \prod_{i=1}^n p_i g_i(\psi'_{i,\tau}), \quad (11)$$

where $g_i(\psi'_{i,\tau}) = 1 - \Phi_i^{(s)}(px_i + 1 - p, py_i + 1 - p)$. Here we show the calculating process by using three networks (1–3) with two connecting bi-directional dependency links: $1 \leftrightarrow 2$ and $2 \leftrightarrow 3$. According to Eq. (8), the fractions of the final remaining nodes in these three networks are $\psi'_{1,\tau} = p_1 r_{21,\tau} g_2(\psi'_{2,\tau})$, $\psi'_{2,\tau} = p_2 r_{12,\tau} g_1(\psi'_{1,\tau}) r_{32,\tau} g_3(\psi'_{3,\tau})$, and $\psi'_{3,\tau} = p_3 r_{23,\tau} g_2(\psi'_{2,\tau})$, respectively. We compute the value of $r_{21,\tau} = p_2 r_{32,\tau} g_3(\psi'_{3,\tau})$ and get $r_{32,\tau} = p_3$ according to Eq. (9). Thus the size of the final GSCC is $p^{(s)}_\infty = \psi'_{1,\tau} g_1(\psi'_{1,\tau}) = \prod_{i=1}^3 p_i g_i(\psi'_{i,\tau})$.

For simplification, we introduce two new variables,

$$z_{i\,\text{in}} = \psi'_{i,\tau}x_i + 1 - \psi'_{i,\tau}, \quad z_{i\,\text{out}} = \psi'_{i,\tau}y_i + 1 - \psi'_{i,\tau}. \quad (12)$$

Substituting Eq. (12) in Eq. (5), we get

$$\psi'_{i,\tau} = \frac{1 - z_{i\,\text{in}}}{1 - \Phi_{i1}(z_{i\,\text{in}}, 1)} = \frac{1 - z_{i\,\text{out}}}{1 - \Phi_{i1}(1, z_{i\,\text{out}})}. \quad (13)$$

Using Eq. (13) and $p^{(s)}_\infty = \psi'_{i,\tau}g_i(\psi'_{i,\tau})$ we obtain

$$p^{(s)}_\infty = \frac{(1 - z_{i\,\text{in}})[1 - \Phi_i^{(s)}(z_{i\,\text{in}}, z_{i\,\text{out}})]}{1 - \Phi_{i1}(z_{i\,\text{in}}, 1)}. \quad (14)$$

When n coupled networks follow the same degree distribution, $\Phi_i^{(s)} = \Phi^{(s)}$ and $\Phi_{i1} = \Phi_1^{(s)}$ for $i = 1, 2, \ldots, n$. Without loss of generality, we set $p_i = p$ for $i = 1, 2, \ldots, n$. We

simplify Eqs. (14) and (11) to be

$$p_\infty^{(s)} = \frac{(1 - z_{in})[1 - \Phi^{(s)}(z_{in}, z_{out})]}{1 - \Phi_1(z_{in}, 1)}, \quad (15)$$

where z_{in} and z_{out} satisfy

$$\frac{1}{p^n} = \frac{[1 - \Phi^{(s)}(z_{in}, z_{out})]^{n-1}[1 - \Phi_1(z_{in}, 1)]}{1 - z_{in}}$$

$$= \frac{[1 - \Phi^{(s)}(z_{in}, z_{out})]^{n-1}[1 - \Phi_1(1, z_{out})]}{1 - z_{out}}. \quad (16)$$

We denote a function $R(z_{in}, z_{out}) \equiv \frac{1}{p}$. The behavior of the final GSCC size when the fraction of the remaining nodes p after the initial failures varies from 0 to 1 can be solved numerically using the function $R(z_{in}, z_{out})$. When $n > 2$, the critical point p_c^{I} where the size of the final GSCC jumps to zero as p decreasing is

$$p_c^{I} = \sqrt[n]{\frac{1 - z_{out}^c}{[1 - \Phi^{(s)}(z_{in}^c, z_{out}^c)][1 - \Phi_1(1, z_{out}^c)]}}, \quad (17)$$

where z_{in}^c and z_{out}^c satisfy

$$\partial_{z_{in}} R(z_{in}^c, z_{out}^c) = 0,$$

$$\partial_{z_{out}} R(z_{in}^c, z_{out}^c) = 0. \quad (18)$$

We next show the results when applying this analytic framework to treelike networks of directed ER, RR, and SF networks.

A. Treelike network of *n* directed ER networks

We construct a treelike network composed of n directed ER networks in which each network i follows a Poisson degree distribution with average degree $\langle k_i \rangle$ with the generating function,

$$\Phi_i(x, y) = e^{(\langle k_i \rangle/2)(x+y-2)}. \quad (19)$$

Since the in degree and out degrees of each ER network node are independent, $\Phi_i(x, y)$ is equivalent to $\Phi_i(x, x)$. The generating functions for computing the size of the GSCC of a single ER network are

$$\Phi_i^{(s)}(x) = 2e^{(\langle k_i \rangle/2)(x-1)} - e^{\langle k_i \rangle(x-1)},$$

$$\Phi_{i1}^{(s)}(x) = e^{(\langle k_i \rangle/2)(x-1)}. \quad (20)$$

Substituting the generating functions of ER networks Eq. (20) into Eq. (11), the size of the final GSCC in the interdependent directed ER networks after removing a fraction of nodes $1 - p_i$ from each network i is

$$p_\infty^{(s)} = \prod_{i=1}^{n} p_i (1 - e^{(\langle k_i \rangle/2)(z_i-1)})^2, \quad (21)$$

where z_i satisfies

$$\frac{1 - z_i}{1 - e^{(\langle k_i \rangle/2)(z_i-1)}} = p_i \prod_{j=1, j \neq i}^{n} p_j (1 - e^{(\langle k_j \rangle/2)(z_j-1)})^2. \quad (22)$$

When the average degree of all the n networks is the same, i.e., $k_i = k$, the size of the final GSCC can be reduced to

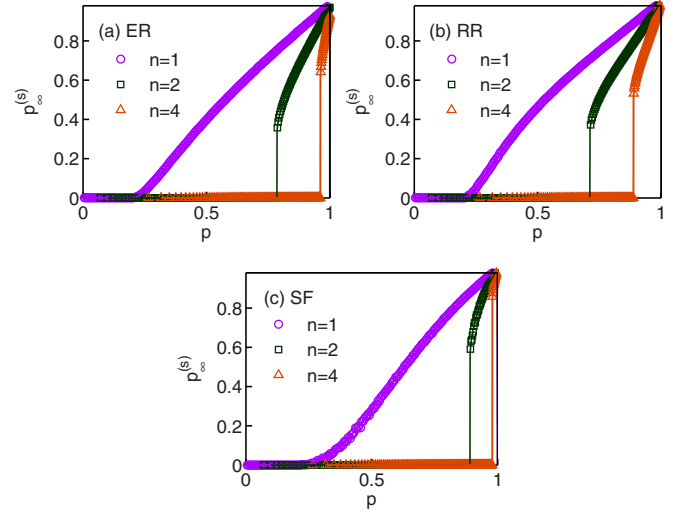$$p_\infty^{(s)} = (1 - z)(1 - e^{(\langle k \rangle/2)(z-1)}), \quad (23)$$

FIG. 2. The percolation behaviors of treelike networks of (a) ER networks ($\langle k \rangle = 10$), (b) RR networks ($k = 10$), and (c) SF networks ($\lambda = 2.5$). For a single network ($n = 1$), the size of the final GSCC continuously decreases to zero when the fraction of remaining nodes p decreases. When the system composes more than two networks ($n \geqslant 2$), the size of the final GSCC discontinuously jumps to zero at a critical point p_c^{I}. The symbols represent simulation results (each network layer contains $N = 10^6$ nodes), the solid lines are theoretic results, and they agree well with each other.

where z is determined by

$$R(z) \equiv \frac{1}{p} = \sqrt[n]{\frac{(1 - e^{(\langle k \rangle/2)(z-1)})^{2n-1}}{(1 - z)}}. \quad (24)$$
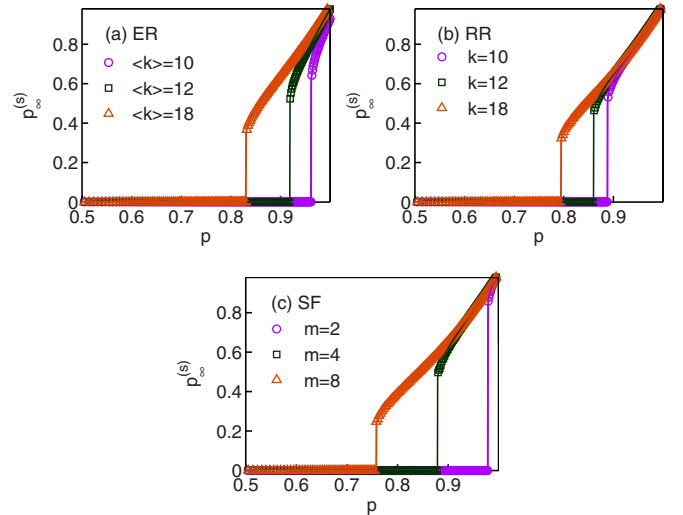

FIG. 3. The final GSCC sizes of the treelike networks of (a) the ER networks with different average degrees, (b) the RR networks with different degrees, and (c) the SF networks ($\lambda = 2.5$) with different minimum in degrees and out degrees. The system contains $n = 4$ networks. The theoretic results (solid lines) agree well with the simulation results (symbols). When the fraction of remaining nodes p changes, these systems all show first order phase transitions.
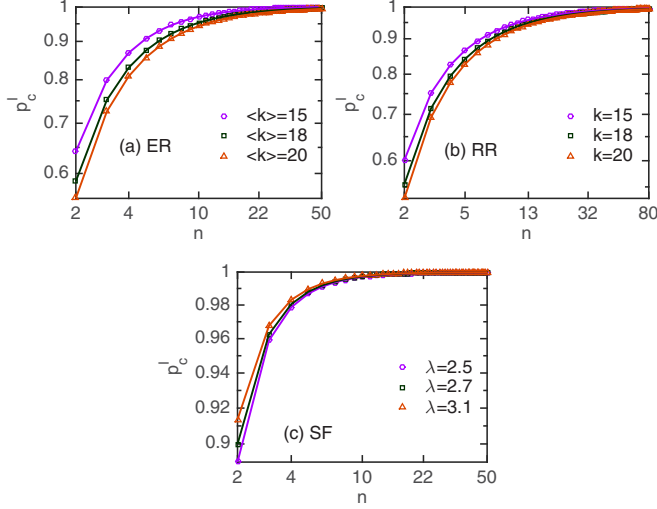
FIG. 4. The critical point p_c^{I} of treelike networks of n (a) ER networks with different average degrees $\langle k \rangle$, (b) RR networks with different degrees k, and (c) SF networks with different degree distribution exponents λ. The results of the ER networks and the RR network are computed by Eqs. (28) and (34), respectively. The results of the SF networks are computed by substituting Eq. (37) with Eq. (17). They are in good agreement with simulations. As more networks are added in, the critical point p_c^{I} increase, indicating the more vulnerable the system is.

Figures 2(a) and 3(a) show that the analytic solutions of Eq. (23) agree with the simulation results. When $n = 1$, the final GSCC size shows a continuous second order phase transition, which is the same as in single directed networks [50]. When $n \geqslant 2$, the system shows a discontinuous first order phase transition at a percolation threshold p_c^{I}. We next calculate the percolation threshold p_c^{I} in treelike networks of ER networks.

For simplicity, we define $\phi_\infty = 1 - z$, then Eq. (23) can be rewritten

$$p_\infty^{(s)} = \frac{[1 - e^{-(\langle k \rangle/2)\phi_\infty}]^{(2n-1)/n}}{\phi_\infty^{1/n}}. \tag{25}$$

According to Eq. (24) and because at the critical point $R'(z) = 0$, the final GSCC size satisfies

$$e^{-(\langle k \rangle/2)\phi_\infty^c} = \frac{1}{(2n-1)\frac{\langle k \rangle}{2}\phi_\infty^c + 1}. \tag{26}$$

When $w = -\frac{\langle k \rangle}{2}\phi_\infty^c - \frac{1}{2n-1}$, Eq. (26) can be simplified

$$\frac{-1}{2n-1}e^{-1/(2n-1)} = we^w. \tag{27}$$

The percolation threshold p_c^{I} in Eq. (17) can be simplified to be

$$p_c^{\mathrm{I}} = \sqrt[n]{\frac{-w}{\frac{\langle k \rangle}{2}\{1 + 1/[(2n-1)w]\}^{2n-2}}}. \tag{28}$$

Figure 4(a) shows the percolation threshold p_c^{I} as a function of the number of networks n. The percolation threshold p_c^{I} increases as n increases, indicating that the greater the number of networks in the system, the more vulnerable the system.
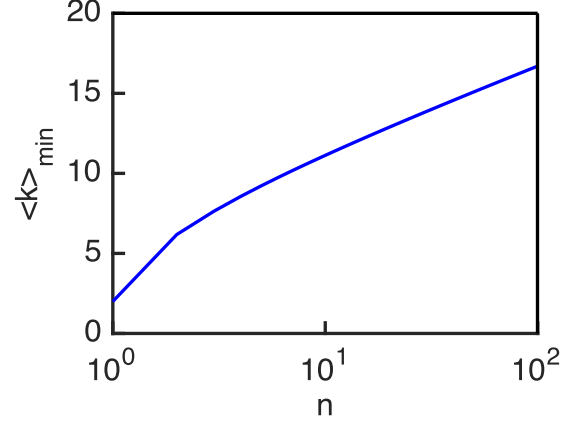

FIG. 5. The minimum average degree $\langle k \rangle_{\min}$ in treelike networks of n ER networks. The treelike networks of the ER networks with $\langle k \rangle < \langle k \rangle_{\min}$ completely collapse even when no node is removed ($p = 1$).

In treelike networks of ER networks there is a minimum average degree $\langle k \rangle_{\min}$ such that when $\langle k \rangle < \langle k \rangle_{\min}$ the system collapses even if no node is removed ($p = 1$). The minimum average degree is determined by the condition $p_c^{\mathrm{I}} = 1$, i.e.,

$$\langle k \rangle_{\min} = \frac{-2w}{\{1 + 1/[(2n-1)w]\}^{2n-2}}. \tag{29}$$

Figure 5 shows that in isolated ER networks ($n = 1$) there is a GSCC when the average degree $\langle k \rangle \geqslant \langle k \rangle_{\min} = 2$ that confirms the result in Ref. [50]. In interdependent networks ($n = 2$) we solve Eqs. (27) and (29) and obtain $\langle k \rangle_{\min} = 6.1783$, which is the same as the result in Ref. [49]. When $n \to \infty$,

$$\langle k \rangle_{\min} = 2\ln(2n-1) + 2O[\ln(2n-1)]. \tag{30}$$

B. Treelike network of n directed RR networks and SF networks

We next apply the analytic framework to treelike networks of directed RR networks [38] and SF networks [52]. In a RR network, the in degree and out degree of each node are the same, and the degree of all nodes is the same. The generating functions for computing the GSCC of a RR network with degree k are

$$\Phi^{(s)}(x) = 2x^{k/2} - x^k,$$
$$\Phi_1^{(s)}(x) = x^{k/2}. \tag{31}$$

In a network of n RR networks with the same degree k, we obtain the final GSCC of the system after cascading failure by substituting Eq. (31) into Eq. (15),

$$p_\infty^{(s)} = (1 - z)(1 - z^{k/2}), \tag{32}$$

where z satisfies

$$R(z) \equiv \frac{1}{p} = \sqrt[n]{\frac{(1 - z^{k/2})^{2n-1}}{1 - z}}. \tag{33}$$

Figures 2(b) and 3(b) show the final GSCC size of a network of n interdependent RR networks. The theoretical results (solid lines) of Eq. (32) agree with the simulation results (symbols). When the fraction of remaining nodes after initial

failure p varies from one to zero, the size of the final GSCC discontinuously jumps to zero at a critical value of p_c^I, which is determined by

$$p_c^I = \sqrt[n]{\frac{1 - z_c}{\left(1 - z_c^{k/2}\right)^{2n-1}}}, \tag{34}$$

where z_c satisfies

$$R'(z_c) = \frac{1 - z_c^{k/2} - (2n-1)\frac{k}{2}z_c^{(k/2)-1}(1 - z_c)}{n}$$
$$\times \sqrt[n]{\frac{\left(1 - z_c^{k/2}\right)^{n-1}}{(1 - z_c)^{n+1}}} = 0. \tag{35}$$

Figure 4(b) shows the critical value of p_c^I as a function of network size n. As in ER networks, when n increases, p_c^I increases, indicating that the greater the number of networks, the more vulnerable the system.

For a directed SF network with no correlation between the in degree and out degree of a given node, the generating function of the degree distribution is

$$\Phi(x, y) = \frac{\sum_{m_{in}}^{M_{in}} \left[(k_{in} + 1)^{1-\lambda_{in}} - k_{in}^{1-\lambda_{in}}\right] x^{k_{in}}}{\left[(M_{in} + 1)^{1-\lambda_{in}} - m_{in}^{1-\lambda_{in}}\right]}$$
$$\times \frac{\sum_{m_{out}}^{M_{out}} \left[(k_{out} + 1)^{1-\lambda_{out}} - k_{out}^{1-\lambda_{out}}\right] y^{k_{out}}}{\left[(M_{out} + 1)^{1-\lambda_{out}} - m_{out}^{1-\lambda_{out}}\right]}, \tag{36}$$

where m_{in} and M_{in} are the minimum and maximum in degrees, respectively, m_{out} and M_{out} are the minimum and maximum out degrees of the SF network, respectively, and λ_{in} and λ_{out} are the power-law exponents of the in-degree distribution and out-degree distribution, respectively. The generating function for computing the GSCC of a SF network is

$$\Phi^{(s)}(x) = \frac{2 \sum_m^M \left[(k+1)^{1-\lambda} - k^{1-\lambda}\right] x^k}{\left[(M+1)^{1-\lambda} - m^{1-\lambda}\right]^2}$$
$$- \frac{\left\{\sum_m^M \left[(k+1)^{1-\lambda} - k^{1-\lambda}\right] x^k\right\}^2}{\left[(M+1)^{1-\lambda} - m^{1-\lambda}\right]^2},$$
$$\Phi_1(x, 1) = \Phi_1(1, x)$$
$$= \frac{\sum_m^M \left[(k+1)^{1-\lambda} - k^{1-\lambda}\right] x^k}{(M+1)^{1-\lambda} - m^{1-\lambda}}. \tag{37}$$

By substituting Eq. (37) into Eq. (14) we numerically calculate the final GSCC sizes of the treelike networks of SF networks. Figures 2(c) and 3(c) show that the analytic results agree with the simulation results. Figures 4(b) and 4(c) show the percolation thresholds of the RR and SF network systems, which again indicates that systems become more vulnerable when they encompass a greater number of networks.

V. RANDOM REGULAR NETWORK OF INTERDEPENDENT DIRECTED NETWORKS

We here apply the analytic framework to RR networks of n interdependent networks that display loops. In a RR network of networks, each network node depends on the same l of other networks. Figure 1(d) shows when each network depends on two neighboring networks. Figure 1(e) shows
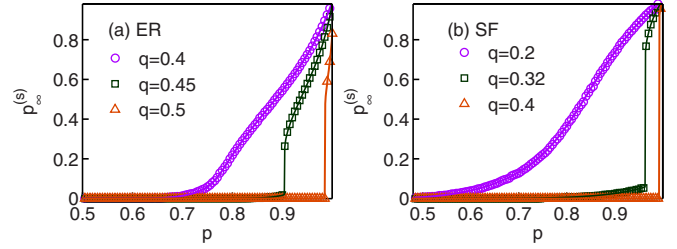

FIG. 6. Percolation behavior of the RR networks of (a) the ER networks ($\langle k \rangle = 15$) and (b) the SF network ($\lambda = 2.5$) with different coupling strengths q and $l = 3$. For both RR networks of the ER networks and RR networks of the SF networks, systems show second order, hybrid, and first order phase transitions with different coupling strengths q. The solid lines represent theoretic results, and they are in perfect agreement with the simulation results (symbols). In simulations, each layer network contains 10^6 nodes, and each data point is averaged over 30 realizations.

when each network depends on three neighboring networks. For simplicity and without loss of generality, we assume that the coupling strengths between each pair of networks are the same, $q_{ij} = q$, and we remove a fraction of nodes $1 - p$ from each network. We here assume that all the networks in the system follow the same degree distribution and the same generating function $g_i(\psi_\tau') = g(\psi_\tau')$ and that there are no correlations between the in-degree and out-degree distributions. Because of the symmetry among all networks, the sizes of the final GSCCs of all the networks is the same, i.e., $\psi_{i,\tau}' = \psi_\tau'$ and $r_{ij,\tau} = r_\tau$. We simplify the equations of the final GSCC size, Eqs. (8) and (9), to

$$\psi_\tau' = p[qr_\tau g(\psi_\tau') - q + 1]^l,$$
$$r_\tau = p[qr_\tau g(\psi_\tau') - q + 1]^{l-1}. \tag{38}$$

When the in-degree and out-degree distributions are independent, Eq. (4) can be written as $g_i(p) = 1 - \Phi_i^{(s)}[px(p) + 1 - p, px(p) + 1 - p]$, and Eq. (5) can be simplified to be $x(p) = \Phi_{i1}[px(p) + 1 - p, 1]$. We substitute $z = px(p) + 1 - p$ into Eq. (10), and the size of the final GSCC becomes

$$p_\infty^{(s)} = \frac{(1 - z)[1 - \Phi^{(s)}(z, z)]}{1 - \Phi_1(z, 1)}, \tag{39}$$

where z satisfies

$$R(z, q) \equiv \frac{1}{p} = \frac{1 - \Phi_1(z, 1)}{1 - z} \left[\frac{1 - q + \sqrt{(1-q)^2 + 4qp_\infty}}{2}\right]^l. \tag{40}$$

For any parameters q and p, and using the generating function of the degree distribution of each network layer, we obtain the value of z by solving Eq. (40). We then substitute z into Eq. (39) to get the size of the final GSCC. Figure 6 shows that the theoretical solution of the final GSCC in the RR network of the ER networks and the RR network of the SF networks both agree with the simulation results.

Under different coupling strengths q, the RR network of the ER networks and the RR network of the SF networks exhibit different phase transitions. For example, when $q = 0.4$ for the ER networks and $q = 0.2$ for the SF networks, the
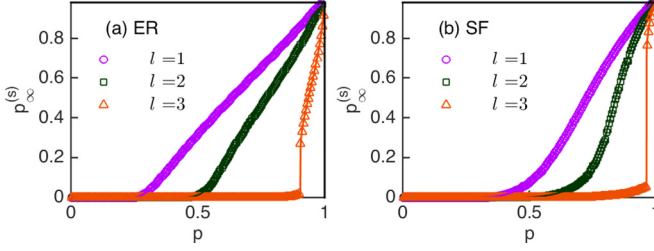
FIG. 7. The final GSCC size of the RR networks of (a) ER networks with $\langle k \rangle = 15$ and $q = 0.45$, and (b) SF networks with $\lambda = 2.5$ and $q = 0.32$. When the degree of every network of the RR network equals one, the system contains a single network and shows a second order phase transition. As l increases, the system becomes more vulnerable. The solid lines represent theoretic results, and they are in perfect agreement with the simulation results (symbols, $N = 10^6$ and averaged over 30 realizations).

size of the final GSCC continuously decreases to zero at a percolation threshold of p_c^{II} as p decreases, showing a second order phase transition [Fig. 6, purple circle]. When $q = 0.5$ for the ER networks and $q = 0.4$ for the SF networks, the size of the final GSCC jumps to zero at another percolation threshold of p_c^{I} as p decreases, showing a first order phase transition [Fig. 6, red triangle]. When $q = 0.45$ for the ER networks and $q = 0.32$ for the SF networks, the size of the final GSCC first jumps to a very small nonzero value at p_c^{I} and then continuously decreases to zero at p_c^{II}, showing a hybrid phase transition [Fig. 6, green square]. In addition, the phase transitions are different in the RR networks of networks with different degrees l (see Fig. 7). The system becomes more vulnerable as l increases.

The percolation thresholds p_c^{I} and p_c^{II} are the physically meaningful extrema of $R(z, q)$ as a function of z, which can be either computed by $dR(z, q)/dz = 0$ or determined by $\lim_{z \to 1} R(z, q)$.

(i) When the system exhibits a second order phase transition, $R(z, q)$ is a monotonically increasing function of z [Fig. 8, cyan solid line], and the maximum value of $R(z, q)$ is obtained when $z \to 1$, which corresponds to the reciprocal of percolation threshold of p_c^{II}. In addition, for the hybrid phase [Fig. 8, red dashed line], $R(z, q)$ is a nonmonotonic increasing function of z, but the maximum value of $R(z, q)$ is also obtained when $z \to 1$, corresponding to the reciprocal of percolation threshold of p_c^{II}. Thus the percolation threshold of p_c^{II} becomes

$$p_c^{\mathrm{II}} = \frac{1}{\lim_{z \to 1} R(z, q)} = \frac{1}{\Phi_1'(1, 1)(1 - q)^l}. \quad (41)$$

(ii) When the system displays a hybrid or a first order phase transition, $R(z, q)$ as a function of z has a peak at z_c [Fig. 8, blue dashed-dotted line], where z_c is a root of $F(z_c, q) = 0$, and $F(z, q) = \partial_z R(z, q)$. The percolation threshold of p_c^{I} is

$$p_c^{\mathrm{I}} = \frac{1}{R(z_c, q)}. \quad (42)$$

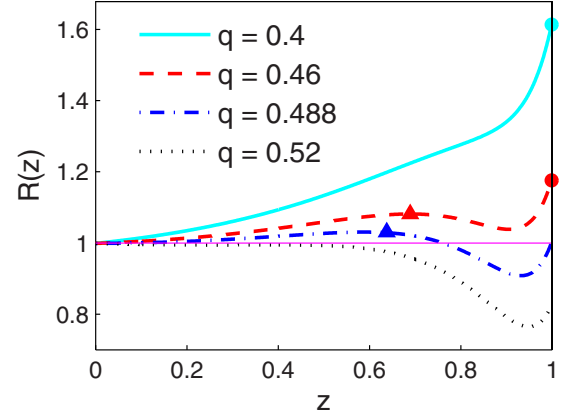We next calculate the critical coupling strengths q_{c1}, q_{c2}, and $q_{\max}$.

FIG. 8. The solution of $R(z, q)$ as a function of z in the RR networks of the ER networks with different coupling strengths q, where $\langle k \rangle = 15$ and each network node has three neighbors. When $q < q_{c2} = 0.4348$, $R(z, q)$ is a nondecreasing function of z, and when $z \to 1$, $R(z, q)$ reaches its maximum value as the cyan solid line shows. When $q_{c2} < q < q_{c1} = 0.4826$, $R(z, q)$ shows a peak in the region $z \in (0, 1)$ (red triangle), but the maximum value continues to be $\lim_{z \to 1} R(z, q)$ as the red dashed line shows. When $q_{c1} < q < q_{\max} = 0.5136$, $R(z, q)$ shows a peak (blue triangle), and the peak value is also its maximum value as the blue dashed-dotted line shows. When $q \geqslant q_{\max}$, $R(z, q) \leqslant 1$ for all the $z \in [0, 1]$ as the black dot line shows. The magenta solid line shows the reference line of $R(z, q) = 1$. The cyan circle and the red circle represent the percolation threshold of $p_c^{\mathrm{II}} = 1/\lim_{z \to 1} R(z, q)$, and the red triangle and blue triangle represent another percolation threshold $p_c^{\mathrm{I}} = 1/R(z_c)$, where z_c is the critical point where the peak appears.

(i) The critical coupling strength q_{c2} separates the second order and hybrid phase transitions. The cyan solid line in Fig. 8 indicates that $R(z, q)$ monotonically increases as z increases in the region of a second order phase transition, i.e., $F(z, q) \geqslant 0$ for any $z \in [0, 1]$. In the region of a hybrid phase transition, $R(z, q)$ has a peak at z_c, i.e., $F(z_c, q) = 0$, as shown in Fig. 8. Thus at the critical coupling strength q_{c2}, the function $F(z, q) = 0$ has only one solution $z = z_{vc}$, which can be guaranteed only when $F(z_{vc}, q_{c2}) = \partial_z F(z, q)|_{z=z_{vc}, q=q_{c2}} = 0$. Thus the critical point q_{c2} is

$$F(z_{vc}, q_{c2}) = 0,$$
$$\partial_z F(z, q)|_{z=z_{vc}, q=q_{c2}} = 0. \quad (43)$$

(ii) The critical coupling strength q_{c1} separates the hybrid and first order phase transitions. Figure 8 shows a peak at $z = z_{fc}$, which is the smaller root of $F(z_{fc}, q) = 0$ in both the first order and the hybrid phase transitions, but the two differ because, in the region of a first order phase transition, $R(z_{fc}, q)$ is the maximum value of the function $R(z, q)$ for $z \in [0, 1]$, whereas, in the region of a hybrid phase transition, $R^{(s)}(z_{fc}, q) < \lim_{z \to 1} R(z, q)$. Thus at the critical coupling strength q_{c1}, the system satisfies

$$R^{(s)}(z_{fc}, q_{c1}) = \lim_{z \to 1} R^{(s)}(z, q_{c1}).$$
$$F(z_{fc}, q_{c1}) = 0. \quad (44)$$

(iii) Another critical point $q_{\max}$ appears, above which ($q > q_{\max}$) the system collapses when even a single node is removed
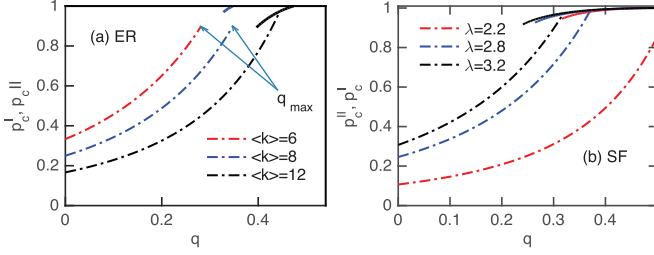
FIG. 9. The percolation thresholds of the RR networks of (a) ER networks with different $\langle k \rangle$'s and (b) SF networks with different λ's. As the coupling strength q increases, the system where each network node has three neighbors shows different phase transitions: (a) The RR networks of the ER networks with small average degrees, such as $\langle k \rangle = 6$, show second order phase transitions until q_{max} is reached where the system suffers from collapse; when the average degree is larger, such as $\langle k \rangle = 8$, the system shows a second order phase transition then changes into a hybrid phase transition and collapse when q_{max} is reached; for even greater average degrees, such as $\langle k \rangle = 12$, the system displays a second order phase transition through a hybrid and then changes into a first order phase transition. (b) For the RR networks of the SF networks with small degree exponents, such as $\lambda = 2.2$, the system shows a second order then a hybrid phase transition and collapse at last. For larger degree exponents, systems undergo a second order through a hybrid to a first order phase transition. The dashed-dotted lines represent the percolation threshold p_c^{II}, and the solid lines are another percolation threshold of p_c^{I}. These two thresholds both appear under the same q, meaning the system shows a hybrid phase transition.

from each network. In the collapsed regions, the function $R^{(s)}(z_{mc}, q_{max}) < 1$ for $z \in [0, 1]$ as with $q = 0.52$ in Fig. 8. The critical point q_{max} separates the first order phase transition and the collapsed regions determined by

$$R^{(s)}(z_{mc}, q_{max}) = 1,$$
$$F(z_{mc}, q_{max}) = 0. \quad (45)$$

Figure 8 shows that function $R(z, q)$ equals 1 when $z = 0$ because the failure of even a single node collapses the system. Thus the critical coupling strength q_{max} is

$$F(z, q_{max})|_{z \to 0} = 0. \quad (46)$$

We next calculate the sizes of the final GSCC $p_\infty^{(s)}$, the percolation thresholds of p_c^{I} and p_c^{II}, the critical coupling strengths q_{c1} and q_{c2}, and q_{max} in the RR networks of the ER networks and the RR networks of the SF networks.

Substituting the generating functions for calculating the size of a single ER network of Eq. (19) into Eqs. (39) and (40), we obtain the size of the final GSCC of the interdependent directed ER networks,

$$p_\infty^{(s)} = (1 - z)(1 - e^{(\langle k \rangle/2)(z-1)}), \quad (47)$$

where z satisfies

$$R^{(s)}(z, q) = \frac{1}{p} = \frac{(1 - e^{(\langle k \rangle/2)(z-1)})[1 - q + \sqrt{(1-q)^2 + 4q(1-z)(1 - e^{(\langle k \rangle/2)(z-1)})}]^l}{2^l(1-z)}. \quad (48)$$

Substituting Eq. (48) into Eqs. (41) and (42), we obtain the percolation thresholds of p_c^{I} and p_c^{II} of the RR network of the ER networks. Figure 9(a) shows that the percolation threshold of p_c^{II} (dashed-dotted line) increases as the coupling strength q increases and disappears at the critical strength q_{c1} or q_{max}. Note that in ER networks with the same average degree $\langle k \rangle$ we have

$$p_c^{II} = \frac{2}{\langle k \rangle (1 - q)^l}. \quad (49)$$

The percolation threshold of p_c^{I} (solid line) appears at critical strength q_{c2} and then increases as q increases. To calculate percolation thresholds of p_c^{I} and p_c^{II}, critical coupling strengths q_{c1} and q_{c2} and q_{max} in the RR networks of the ER networks, we determine the derivation function $F(z, q)$ of the function $R^{(s)}(z, q)$,

$$F(z, q) \equiv \frac{dR^{(s)}(z, q)}{dz}$$
$$= \frac{e^{(\langle k \rangle/2)(1-z)} - \frac{\langle k \rangle}{2}(1 - z) - 1}{p(1 - z)(e^{(\langle k \rangle/2)(1-z)} - 1)} - \frac{2ql\{e^{(\langle k \rangle/2)(z-1)}[\frac{\langle k \rangle}{2}(1 - z) - 1] + 1\}}{p(1 - q + a^{(s)})a^{(s)}}, \quad (50)$$

where a satisfies

$$a^{(s)} = \sqrt{(1-q)^2 + 4q(1-z)(1 - e^{(\langle k \rangle/2)(z-1)})}. \quad (51)$$

By solving z_c from $F(z_c, q) = 0$ for each coupling strength q we get another percolation threshold,

$$p_c^{I} = \frac{2^l(1 - z_c)}{(1 - e^{(\langle k \rangle/2)(z_c-1)})[1 - q + \sqrt{(1-q)^2 + 4q(1-z_c)(1 - e^{(\langle k \rangle/2)(z_c-1)})}]^l}. \quad (52)$$

We obtain the critical coupling strengths q_{c1}, q_{c2}, and q_{max} by substituting Eqs. (50) and (51) into Eqs. (43)–(45),

respectively. Figure 10(a) shows the phase diagram of the RR network of the ER networks where each network depends on
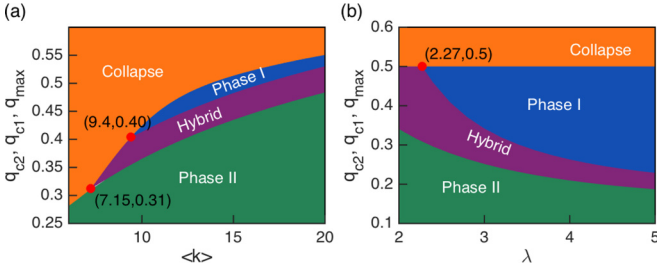
FIG. 10. Phase diagrams of the random regular networks of (a) the ER networks and (b) the SF networks where each network node has three neighbors. The green region labeled Phase II is the region of the second order phase transition. The purple region labeled Hybrid is the region of the hybrid phase transition. The blue region labeled Phase I is the region of the first order phase transition. The orange region labeled Collapse is the region where the system collapse even without removing nodes. Triple points (red dots) appear in the phase diagram.

three neighboring networks, the curve separates the region of the second order phase transition (the green region labeled "Phase II"), and the region of the hybrid phase transition (the purple region labeled Hybrid) is the critical strength q_{c2} under different average degrees $\langle k \rangle$. The curve of the critical strength q_{c1} separates the hybrid phase transition and the first order phase transition (the blue region labeled "Phase I"), and the critical strength q_{max} separates the first order phase transition and the region of collapse (the orange region labeled "Collapse"). These three critical strengths increase as the average degree $\langle k \rangle$ increases, indicating that the more dense the ER network, the more robust the system. A triple point intersected by regions of Phase I, Hybrid, and Collapse and another triple point intersected by regions of Phase II, Hybrid, and Collapse appear in the phase diagram, which is a quantitative index that enables us to design robust systems far from the collapse region.

Computing the size of the final GSCC, the percolation thresholds, and the critical coupling strengths in the RR networks of the SF networks is similar to the procedure for the RR networks of the ER networks. We substitute the generating function Eq. (37) for calculating the size of a single SF network into Eqs. (39) and (40) and obtain the size of the final GSCC in interdependent directed ER networks and the function $R^{(s)}(z, q)$. Using the function $R^{(s)}(z, q)$ and its derivation, we calculate percolation thresholds of p_c^{I} and p_c^{II} in Fig. 9(b) and the critical coupling strengths q_{c1}, q_{c2}, and q_{max} in Fig. 10(b). Note that when using Eqs. (39) and (40) to calculate the critical coupling strength q_{max} we rewrite the function $F(z, q)$ to be

$$
\begin{aligned}
F(z, q) = {} & \frac{-\Phi_1'(z, 1)R(z, q)}{1 - \Phi_1(z, 1)} + \frac{R(z, q)}{1 - z} \\
& + \frac{2l R(z, q)}{1 - q + \sqrt{(1 - q)^2 + 4q p_\infty^{(s)}}} \\
& \times \frac{q p_\infty'}{\sqrt{(1 - q)^2 + 4q p_\infty^{(s)}}}.
\end{aligned}
\tag{53}
$$

When $q = q_{max}$, $p_\infty^{(s)}|_{z \to 0} = 1$, and $p_\infty^{(s)}|_{z \to 0} = -1$. We solve Eq. (46) and obtain

$$
q_{max} = \frac{1}{l - 1}.
\tag{54}
$$

Note that the q_{max} for the RR network of the directed SF networks is the same as that for the RR network of the undirected SF networks [53]. Figure 10(b) shows that for the RR network of the SF networks with $l = 3$ where each SF network depends on three neighboring networks, $q_{max} = 0.5$. In the phase diagram of the RR network of the SF networks there are triple points intersected by regions labeled Phase I, Hybrid, and Collapse that help us understand the robustness mechanisms and suggest ways of pushing the system into a safe region. In addition, the other critical coupling strengths q_{c1} and q_{c2} decrease as the degree distribution exponent λ increases. Thus in the RR networks of the SF networks, the more heterogenous (smaller λ) the networks, the more robust the system.

VI. CONCLUSION

We have developed a general theoretical framework for analyzing the robustness of networks of directed networks with arbitrary degree distributions and have discovered that the phase diagram of a network of directed networks differs from that of a network of undirected networks. For example, the RR network of a directed ER network shows a hybrid phase transition that is absent in a network of undirected ER networks. We also find that system robustness in directed networks is affected by network topology. The treelike structure of directed networks changes from a second order phase transition to a first order phase transition as coupling strength q increases. An RR network of directed networks shows a second order phase transition when the coupling strength $q < q_{c2}$, a hybrid phase transition when $q_{c2} < q < q_{c1}$, a first order phase transition when $q_{c1} < q < q_{max}$, and collapses when $q > q_{max}$. We also find triple points in the phase diagram of the RR network of both directed ER and directed SF networks. These findings enable us to better understand system robustness and to design more robust infrastructures.

The framework presented in our paper suggests some questions for further study. (i) How do in-degree and out-degree correlations in a network and degree correlations between networks influence system robustness? (ii) The NODN model assumes that nodes in one network are randomly dependent on nodes in other networks, but in real-world systems interdependent relations are not random. How do we study robustness in real-world networks of networks? Answering these questions will expand our understanding of robustness in interdependent complex systems.

[1] A.-L. Barabási and R. Albert, Science **286**, 509 (1999).

[2] R. Albert, I. Albert, and G. L. Nakarado, Phys. Rev. E **69**, 025103 (2004).

[3] R. Cohen, K. Erez, D. ben-Avraham, and S. Havlin, Phys. Rev. Lett. **85**, 4626 (2000).

[4] M. Faloutsos, P. Faloutsos, and C. Faloutsos, in *ACM SIG-COMM Computer Communication Review*, Vol. 29 (ACM, New York, 1999), pp. 251–262.

[5] R. Cohen, K. Erez, D. ben-Avraham, and S. Havlin, Phys. Rev. Lett. **86**, 3682 (2001).

[6] D. S. Callaway, M. E. J. Newman, S. H. Strogatz, and D. J. Watts, Phys. Rev. Lett. **85**, 5468 (2000).

[7] R. Albert and A.-L. Barabási, Rev. Mod. Phys. **74**, 47 (2002).

[8] H. Jeong, B. Tombor, R. Albert, Z. N. Oltvai, and A.-L. Barabási, Nature (London) **407**, 651 (2000).

[9] X. Liu and L. Pan, BMC Syst. Biol. **8**, 51 (2014).

[10] X. Liu and L. Pan, IEEE/ACM Trans. Comput. Biol. Bioinf. **12**, 467 (2015).

[11] R. Albert, H. Jeong, and A.-L. Barabási, Nature (London) **406**, 378 (2000).

[12] R. Cohen and S. Havlin, *Complex Networks: Structure, Robustness and Function* (Cambridge University Press, Cambridge, UK, 2010) .

[13] S. V. Buldyrev, R. Parshani, G. Paul, H. E. Stanley, and S. Havlin, Nature (London) **464**, 1025 (2010).

[14] D. Cellai, E. López, J. Zhou, J. P. Gleeson, and G. Bianconi, Phys. Rev. E **88**, 052811 (2013).

[15] G. Bianconi and S. N. Dorogovtsev, Phys. Rev. E **89**, 062814 (2014).

[16] J. Gao, X. Liu, D. Li, and S. Havlin, Energies **8**, 12187 (2015).

[17] Y. Moreno, J. Gómez, and A. Pacheco, Europhys. Lett. **58**, 630 (2002).

[18] J. Gómez-Gardenes, Y. Moreno, and L. M. Floría, Biophys. Chem. **115**, 225 (2005).

[19] J. Gao, S. V. Buldyrev, H. E. Stanley, and S. Havlin, Nat. Phys. **8**, 40 (2012).

[20] G. Paul, T. Tanizawa, S. Havlin, and H. E. Stanley, Eur. Phys. J. B **38**, 187 (2004).

[21] F. Radicchi, Phys. Rev. E **91**, 010801 (2015).

[22] E. Leicht and R. M. D'Souza, arXiv:0907.0894.

[23] R. Parshani, S. V. Buldyrev, and S. Havlin, Phys. Rev. Lett. **105**, 048701 (2010).

[24] C. D. Brummitt, R. M. D'Souza, and E. A. Leicht, Proc. Natl. Acad. Sci. USA **109**, E680 (2012).

[25] W. Li, A. Bashan, S. V. Buldyrev, H. E. Stanley, and S. Havlin, Phys. Rev. Lett. **108**, 228702 (2012).

[26] S. Gómez, A. Díaz-Guilera, J. Gómez-Gardeñes, C. J. Pérez-Vicente, Y. Moreno, and A. Arenas, Phys. Rev. Lett. **110**, 028701 (2013).

[27] M. De Domenico, A. Solé-Ribalta, E. Cozzo, M. Kivelä, Y. Moreno, M. A. Porter, S. Gómez, and A. Arenas, Phys. Rev. X **3**, 041022 (2013).

[28] F. Radicchi and A. Arenas, Nat. Phys. **9**, 717 (2013).

[29] K. Zhao and G. Bianconi, J. Stat. Mech. (2013) P05005.

[30] S. Boccaletti *et al.*, Phys. Rep. **544**, 1 (2014).

[31] X. Liu, H. Peng, and J. Gao, Chaos **80**, 125 (2015).

[32] F. Radicchi, Nat. Phys. **11**, 597 (2015).

[33] F. Radicchi and G. Bianconi, Phys. Rev. X **7**, 011013 (2017).

[34] V. Rosato *et al.*, Int. J. Crit. Infrastruct. **4**, 63 (2008).

[35] M. E. J. Newman, S. H. Strogatz, and D. J. Watts, Phys. Rev. E **64**, 026118 (2001).

[36] P. Erdős and A. R&WI, Publ. Math. Debrecen **6**, 290 (1959).

[37] M. Molloy and B. Reed, Random Struct. Algorithms **6**, 161 (1995).

[38] J. Gao, S. V. Buldyrev, S. Havlin, and H. E. Stanley, Phys. Rev. E **85**, 066134 (2012).

[39] J. Gao, S. V. Buldyrev, S. Havlin, and H. E. Stanley, Phys. Rev. Lett. **107**, 195701 (2011).

[40] M. Kivelä, A. Arenas, M. Barthelemy, J. P. Gleeson, Y. Moreno, and M. A. Porter, J. Complex Networks **2**, 203 (2014).

[41] M. De Domenico, V. Nicosia, A. Arenas, and V. Latora, Nat. Commun. **6**, 6864 (2015).

[42] M. De Domenico, C. Granell, M. A. Porter, and A. Arenas, Nat. Phys. **12**, 901 (2016).

[43] E. Segal *et al.*, Nat. Genet. **34**, 166 (2003).

[44] J. R. Banavar, A. Maritan, and A. Rinaldo, Nature (London) **399**, 130 (1999).

[45] P. J. Menck, J. Heitzig, J. Kurths, and H. J. Schellnhuber, Nat. Commun. **5** (2014).

[46] M. E. Newman, Proc. Natl. Acad. Sci. USA **101**, 5200 (2004).

[47] F. E. Walter, S. Battiston, and F. Schweitzer, Autonomous Agents Multiagent Syst. **16**, 57 (2008).

[48] N. Azimi-Tafreshi, S. N. Dorogovtsev, and J. F. F. Mendes, Phys. Rev. E **90**, 052809 (2014).

[49] X. Liu, H. E. Stanley, and J. Gao, Proc. Natl. Acad. Sci. USA **113**, 1138 (2016).

[50] S. N. Dorogovtsev, J. F. F. Mendes, and A. N. Samukhin, Phys. Rev. E **64**, 025101 (2001).

[51] N. Schwartz, R. Cohen, D. ben-Avraham, A.-L. Barabási, and S. Havlin, Phys. Rev. E **66**, 015104(R) (2002).

[52] M. Boguná, R. Pastor-Satorras, and A. Vespignani, Eur. Phys. J. B **38**, 205 (2004).

[53] J. Gao, S. V. Buldyrev, H. E. Stanley, X. Xu, and S. Havlin, Phys. Rev. E **88**, 062816 (2013).